ACS APPLIED BIO MATERIALS

www.acsabm.org Article

Water-Stable Silver-Based Metal–Organic Frameworks of Quaternized Carboxylates and Their Antimicrobial Activity

Bao-Ping Xie,[§] Jin-Wei Chai,[§] Cheng Fan, Ji-Hua Ouyang, Wen-Jun Duan, Bin Sun, Jun Chen, Li-Xia Yuan,* Xue-Qing Xu,* and Jin-Xiang Chen*

Cite This: *ACS Appl. Bio Mater.* 2020, 3, 8525–8531 Read Online

ACCESS | Metrics & More | Article Recommendations | Supporting Information

ABSTRACT: Three-dimensional (3D) and two-dimensional (2D) Ag-based zwitterionic metal–organic frameworks (MOFs) $[Ag_2(Cedcp)]_n$ (**1**, 3D, H_3CedcpBr denotes *N*-(carboxyethyl)-(3,5-dicarboxyl)-pyridinium bromide) and $\{[Ag_4(Cmdcp)_2(H_2O)_4]\cdot 4H_2O\}_n$ (**2**, 2D, H_3CmdcpBr denotes *N*-(carboxymethyl)-(3,5-dicarboxyl)-pyridinium bromide) have been prepared and investigated for antimicrobial activity via minimal inhibition concentration (MIC) test and killing kinetic assay. Both MOFs **1** and **2** show good water stability and solubility ascribed to their characteristic aromatic rings and positively charged pyridinium of the ligands, as well as the presence of Ag^+ on their surface, leading to strong antimicrobial activity and a wide antimicrobial spectrum toward Gram-negative and positive bacteria. The results indicated that MOF **2** possesses a faster antibacterial activity (60 min) than MOF **1** (120 min). Scanning electron microscopy analysis further suggests that the Ag-based MOFs are capable of rupturing the bacterial membrane, leading to cell death. Moreover, both MOFs exhibit little hemolytic activity against mouse erythrocytes and show good biocompatibility *in vitro*, rendering MOFs **1** and **2** potential therapeutic agents for diseases caused by bacteria.

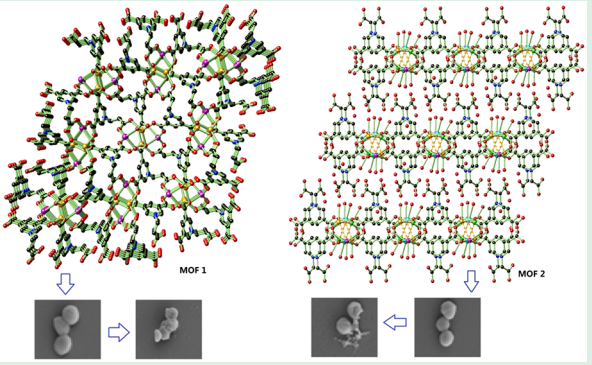

KEYWORDS: *water-stable, silver organic frameworks, crystal structure, antimicrobial activity, killing kinetics assay*

INTRODUCTION

Infectious diseases caused by pathogenic bacteria pose serious concerns to human health, and antibiotics are the simplest and most effective drugs to reduce clinical bacterial infections. However, extensive results have demonstrated that overuse and abuse of antibiotics have led to drug resistance and bacterial imbalance. Particularly, the strong drug resistance produced by bacteria (or "super bacteria") has become a serious issue.[1,2] Thus, it is imperative and urgent to develop effective and environmental-friendly antibacterial materials.

Silver-based inorganic and organic–inorganic composite materials have been widely exploited to show strong inhibitory or bactericidal effects on microbes.[3−7] They have been increasingly used in many normal commodities and medical equipment.[8,9] Lately, some pertinent metal–organic frameworks (MOFs) have also appeared as novel antibacterial agents that exhibit some unique traits including a wide antibacterial spectrum,[10] long periods of persistence,[11] and promising efficacy.[12] Compared to conventional drugs, MOF-based antibacterial agents have many advantages. The active sites of metal ions in the MOFs are effectively wrapped by the organic ligands and evenly distributed across the overall material,[13] enabling a sustained release of metal ions to avoid the toxicity caused by a burst release of metal ions.[14] In 1997, Nomiya et al. presented the first case of Ag-based MOF $[Ag(imd)]_n$ (Himd = imidazole) against bacteria, yeast, and mold.[15] In 2014, Tabar et al. demonstrated that Zn-based MOF prepared from azelaic acid and 4-hydrazinebenzoate mixed ligands exhibited strong antimicrobial properties.[16] The progress of developing antimicrobial MOFs is nevertheless slow due to their water-/buffer- stability and solubility.[17]

In the past few years, we have developed an intense interest in MOFs constructed from quaternized carboxylate ligands due to their good water-dispersity and water-stability. These MOFs have shown promising properties in magnetic resonance imaging,[18] and as probes for nucleic acids,[19−22] metal ion,[23,24] and other biologically relevant species.[25] Herein, we extended our focus on the antibacterial activity of MOFs of quaternized carboxylate ligands by their assembly with Ag^+ ion. A three-dimensional (3D) MOF $[Ag_2(Cedcp)]_n$ (**1**, H_3CedcpBr denotes *N*-(carboxyethyl)-(3,5-dicarboxyl)-pyridi-

Received: July 21, 2020
Accepted: October 27, 2020
Published: November 10, 2020

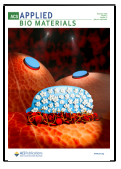

https://dx.doi.org/10.1021/acsabm.0c00896
ACS Appl. Bio Mater. 2020, 3, 8525–8531

nium bromide) and a 2D MOF $\{[Ag_4(Cmdcp)_2(H_2O)_4]\cdot 4H_2O\}_n$ (**2**, H_3CmdcpBr denotes *N*-(carboxymethyl)-(3,5-dicarboxyl)-pyridinium bromide) have been synthesized under mild conditions. MOFs **1** and **2** show good water stability and solubility and strong antimicrobial activity with good biocompatibility.

EXPERIMENTAL SECTION

The synthesis of H_3CmdcpBr was executed following our reported method.[26] Microanalysis data were collected on a Carlo Erba (Italy) EA1110 CHN elemental analyzer. Fourier transform infrared (FT-IR) spectra were collected on a Nicolet (USA) MagNa-IR 550 interferometer. The samples were characterized by Rigaku (Japan) D/max2200/PC powder X-ray diffraction (PXRD, Cu−Kα radiation). The morphological changes of the bacteria were taken using a scanning electron microscope (SEM, JSM-6330F, made by Nippon Electronics Co.). The absorption of bacterial liquid was observed by a microplate spectrophotometer (Tecan, Switzerland, Infinite M200 Pro).

The test microorganisms including *Pseudomon asaeruginose* (ATCC 27853), *Escherichia coli* (ATCC 25922), *Staphylococcus aureus* (ATCC 25923), *Staphylococcus aureus* (ATCC 6538), *Monilia albican* (ATCC 2002), *Propionibacterium acnes* (ATCC 6919), and *Bacillus subtilis* (CMCC 63501) were supplied by Guangdong Institute of Microbiology, and Methicillin-resistant *Staphylococcus aureus* (MRSA 64589) was provided from Nanfang hospitals. The target microbes were cultured in Luria−Bertani broth (LB) and frozen with 20% (W/V) glycerol and stored at −20 °C.

The reagent of *N*,*N*-dimethylformamide (DMF) and $AgNO_3$ was purchased bought from Guangdong Guanghua Sci-Tech Co., Ltd. and Shanghai Fine Chemical Materials Research Institute, respectively. Agar, yeast extract, and Tryptone were purchased from Oxoid Biotechnology Co., Ltd. Ampicillin was bought from Sigma-Aldrich trade Co., Ltd., and 4% glutaraldehyde solution was purchased by Leagene Biotechnology Co., Ltd.

Synthesis of H_3CedcpBr. Powder of 3,5-dicarboxypridine (3.34 g, 20 mmol) was dissolved in DMF (17 mL) and then a DMF (16 mL) solution of bromopropionic acid (3.06 g, 20 mmol) slowly added. The white precipitate formed from the yellow solution slowly and the mixture was further stirred at 65 °C for 18 h. The white solid was obtained by filtration and washed with DMF/acetone (80 mL, *v*:*v* = 1:1) three times. White powder was obtained and dried in vacuum to afford H_3CedcpBr (5.89 g, 92%). Anal. calcd. for $C_{10}H_{10}NO_6Br$: C 37.52, H 3.15, N 4.38; found: C 37.68, H 3.53, N 4.81. IR (KBr disc) ν 3413 (s), 3026 (s), 2502 (m), 1934 (m), 1706 (s), 1647 (s), 1608 (s), 1542 (m), 1429 (s), 1335 (m), 1281 (s), 1259 (s), 1160 (m), 1069 (s), 1005 (s), 815 (s), 750 (s), 630 (s) cm^{-1}. ^1H NMR (400 MHz, D_2O, Figure S1a) δ 9.21 (s, 2H), 9.08 (s, 1H), 4.86 (t, J_1 = 4 Hz, J_2 = 8 Hz, 2H), 2.92 (t, J_1 = 4 Hz, J_2 = 8 Hz, 2H). ^{13}C NMR (100 MHz, D_2O, Figure S1b) δ 176.91, 167.50, 146.10, 144.45, 136.90, 59.06, 37.98.

Synthesis of $[Ag_2(Cedcp)]_n$ (1). H_3CedcpBr (0.3 mmol, 96 mg) in H_2O (5 mL) was neutralized to pH 6.0 using a NaOH solution (0.1 M). $AgNO_3$ (0.6 mmol, 101.9 mg) in H_2O (1.5 mL) was subsequently introduced. The reaction mixture containing white precipitate was heated to dissolve the precipitate and immediately filtered. The filtrate was then allowed to stand at r.t. for 3 days. The colorless crystals of MOF **1** were collected by filtration and dried in vacuum. Yield: 121 mg (89% based on Ag). Anal. calcd. for $C_{10}H_7Ag_2NO_6$: C 26.52, H 1.56, N 3.09; found: C 26.94, H 1.71, N 3.01. IR (KBr disc, cm^{-1}): 3425 (w), 3025 (w), 1643 (m), 1551 (s), 1361 (s), 1225 (m), 1170 (m), 1109 (m), 930 (w), 861 (w), 760 (s), 721 (s), 665 (m), 598 (m), 495 (m), 435 (s).

Synthesis of $\{[Ag_4(Cmdcp)_2(H_2O)_4]\cdot 4H_2O\}_n$ (2). The similar synthesis procedure for MOF **1** was used for MOF **2** using ligand H_3CmdcpBr (0.3 mmol, 92 mg) and $AgNO_3$ (0.6 mmol, 101.8 mg). Yield: 141 mg (92% based on Ag). Anal. calcd. for $C_{18}H_{26}Ag_4N_2O_{20}$: C 21.16, H 2.56, N 2.74; found: C 21.28, H 2.50, N 3.07. IR (KBr disc): 3048 (w), 1640 (m), 1577 (s), 1355 (s), 1285 (m), 1236 (m), 1175 (m), 956 (w), 923 (w), 793 (w), 767 (m), 721 (s), 628 (m), 604 (m), 524 (m), 439 (s) cm^{-1}.

X-ray Crystal Structure Determinations. X-ray structure characterizations of MOFs **1** and **2** were performed on a Bruker APEX II diffractometer equipped with graphite-monochromated irradiation Mo Kα (λ = 0.71073 Å), with absorption correction carried out using SADABS.[27] The crystal structures of **1** and **2** were solved by direct methods and refined against F^2 using full-matrix least-squares techniques with SHELXTL-2013.[28] The coordinates of hydrogen atoms on the water were calculated by the Calc−OH function in WinGX.[29] Crystallographic data of **1** and **2** have been deposited with CCDC (Cambridge Crystallographic Data Center) numbers 2015720 and 2015721. Pertinent crystallographic information for MOF **1** and MOF **2** is tabulated in Table S1, while their selected bond distances (Å) and angles (deg) are listed in Tables S2 and S3, respectively.

Minimal Inhibitory Concentration (MIC) Test. The antimicrobial capability of MOFs **1** and **2** was evaluated by MIC with a two-fold microdilution method. Briefly, after growing in Luria−Bertani (LB) broth at 37 °C to exponential phase, microbes were diluted with fresh LB broth to reach the density of 10^6 CFU/mL. An equal volume of microbial inoculums was added into 96-well microtiter plates with different concentrations of MOFs, which were filtered to remove bacteria before use. Plates were incubated at 37 °C for 16−18 h and the MIC values at which no microbial growth occurred were recorded at 600 nm using a microplate spectrophotometer. All experiments were performed in triplicates with Ampicillin as positive control.

Bactericidal Kinetics Assay. The bactericidal kinetics assay of MOFs **1** and **2** against *S. aureus* ATCC25923 was investigated according to the protocol described in our previous study with slight modification.[30] In brief, *S. aureus* ATCC25923 was collected in the exponential phase, washed twice with PBS, and diluted to 10^6 CFU/mL with fresh LB broth. The microorganisms were treated with a serial concentration of MOF **1** or **2** and incubated at 37 °C. Aliquots at the different time points (0, 15, 30, 60, 90, 120, and 150 min) were coated on LB agar plates, and the bacteria-killing kinetics was determined by the number of viable colonies after cultured at 37 °C for 18 h. Sterile deionized water was used as a negative control.

Scanning Electron Microscopy (SEM) for Morphology Alteration of Microbes Treated with MOFs 1 and 2. The morphology alteration of microbes treated with MOFs **1** and **2** was investigated using scanning electron microscopy (SEM). Briefly, after filtration to remove bacteria, 1 × MIC of MOF **1** or **2** was incubated with logarithmic phase culture of *S. aureus* ATCC 25923 (1×10^7 CFU/mL) for 30 min at 37 °C. The bacteria pellets were collected by centrifuging for 5 min at 3000 rpm and fixed with 4% glutaraldehyde solution at 4 °C for 4 h. After being washed with 0.1 M PBS, the pellets were then fixed again with 2.5% glutaraldehyde solution at 4 °C for 4 h. Cells were sufficiently washed with PBS and dehydrated with a gradation of ethanol concentrations (30%, 50%, 70%, 85%, 90%). After critical point drying and coating with gold, the morphology of the samples was observed and about 5−10 single plane images per sample were acquired.

Hemolysis Assay. Mouse red blood cells (mRBCs) were isolated through centrifugation, rinsed three times with TBS, and then suspended to 2% (*v*/*v*) in TBS. Then 200 μL mRBC suspension was respectively added into a 96-well V-shaped sterilized plate. To each well was added MOF **1** or **2** with different concentration gradient, and the plate was incubated for 3.0 h at room temperature, then centrifuged (1000 g, 5 min). Then 100 μL aliquots of supernatant were transferred to a fresh 96-well plates and hemoglobin release was monitored with a Microplate autoreader (Infinite M1000 Pro) by measuring the absorbance at 540 nm. In 0.1 M PBS and 0.1% SDS, 0% and 100% hemolysis were determined, respectively.

RESULTS AND DISCUSSION

Choice and Characterization of MOFs 1 and 2. Compared with the reported Ag-based MOFs,[31] MOFs **1** and **2** were synthesized in water instead of commonly used

https://dx.doi.org/10.1021/acsabm.0c00896
ACS Appl. Bio Mater. 2020, 3, 8525−8531

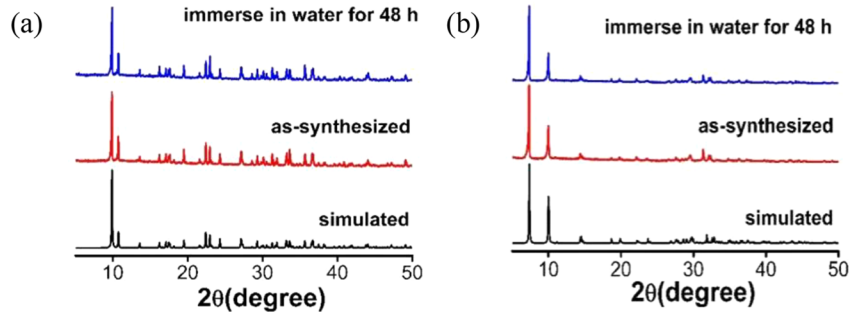

Figure 1. PXRD patterns of MOFs (a) **1** and (b) **2**, showcasing good agreement between the simulated, as-synthesized, and the sample immersing in H_2O for 48 h.

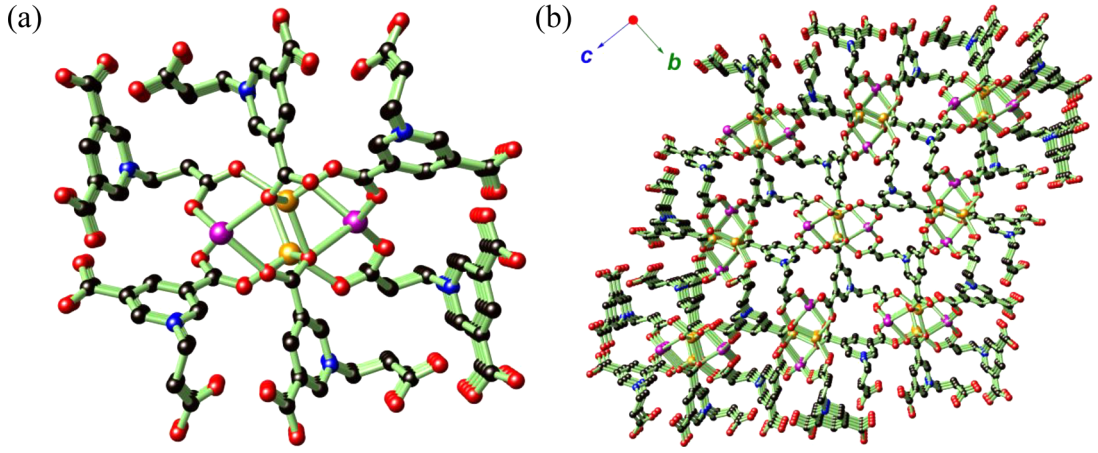

Figure 2. (a) One-dimensional structure formed from Ag^+ and ligands looking down *a* axis. (b) Three-dimensional structure of MOF **1** looking along the *a* axis, color codes: Ag(1) (dark magenta), Ag(2) (orange), O (red), N (blue), and C (black).

organic solvents. It is thus an environmentally benign synthetic method. Upon immersing fresh powder of **1** or **2** in H_2O for 48 h, the powder X-ray diffraction (PXRD) patterns are in good agreement with that generated from single-crystal diffraction data, indicating both bulky phase purity and water stability. The observed water stability of **1** and **2** is likely inherited from the high polarity of their respective ligands (Figure 1). The water-stable nature will contribute to their antibacterial activity study in the buffer. Upon ultrasonication, MOFs **1** and **2** have good solubility in aqua with concentrations of approximately up to 186.83 μM for **1** and 100.43 μM for **2**.

Crystal Structure of $[Ag_2(Cedcp)]_n$ (1). MOF **1** was characterized to crystallize in the orthorhombic space group $P2_12_12_1$, and its asymmetric unit features one independent Cedcp ligand associated with two Ag(I) ions (Ag1 and Ag2, Figure S2a). In **1**, Ag1 exhibits a tetrahedral coordination geometry and is bonded by four Cedcp ligands (Figure S2b), whereas Ag2 is coordinated by five Cedcp ligands to give a triangular bipyramidal geometry (Figure S2c). Ag1 and Ag2 are alternatively aligned and juxtaposed by the Cedcp ligands along the crystallographic *a* direction, yielding Ag1···Ag2 distances of 3.06 and 3.34 Å. These values are lower than the sum of Van Der Waals radius of a pair of Ag^+ (3.44 Å), indicating the Ag1···Ag2 interactions. The Cedcp ligands thus support 1D −[Ag1···Ag2]− chain extended along the *a* direction (Figure 2a and Figure S2d), featuring Cedcp ligands projecting to six directions within the *bc* plane with high connectivity of 12. These Cedcp ligands, in turn, extend the 1D −[Ag1···Ag2]− chain along the *bc* plane to ultimately give a densely packed 3D structure (Figure 2b).

MOF **2** was characterized to crystallize in the triclinic space group *P*−1 and its asymmetric unit features four independent Ag(I) ions bonded to a pair of Cmdcp ligands, with each Ag(I) ion further ligated by one terminal H_2O molecule (Figure S3a). Besides, there also exist four free H_2O molecules in the unit. In **2**, the four Ag(I) can be treated as two similar groups, Ag1 with Ag4, and Ag2 with Ag3. These two groups from their independent cuboidal cluster units with shared geometry and differ only in their relevant bond distances and angles. Therefore, only the cluster unit sustained by Ag1 and Ag4 is featured and that of Ag2 and Ag3 will be discussed when necessary.

In **2**, Ag1/Ag2 adopts a square pyramidal coordinated geometry with its equatorial plane defined by four O atoms from four Cmdcp ligands and capped by one O from H_2O (Figure S3b). Such coordination geometry of Ag1/Ag2 also contrasts that identified in MOF **1** with triangular bipyramidal geometry. In contrast, Ag3/Ag4 exhibits a seesaw-shaped geometry and is associated with three O atoms from Cmdcp ligands and one O from H_2O (Figure S3c).

A distinctive feature of MOF **2** is that its extended structure is based on a discrete cuboidal Ag_4 cluster unit. As shown in Figure S3d, the Ag_4 unit features a pair of Ag1···Ag4 contacts of 2.95 Å, an indication of Ag···Ag interactions. The Ag_4 cubane further features eight Ag−O bonds and two carboxylate (O−C−O) bridges to define its 12 edges. Notably, such Ag_4 cubane, with argentophilicity, might play a structural dictating

https://dx.doi.org/10.1021/acsabm.0c00896
ACS Appl. Bio Mater. 2020, 3, 8525−8531

role, in contrast to those cuboidal clusters such as Ni_4 formed by alternatively arranged Ni and O vertices.[32]

Interestingly, a similar cubane supported by Ag2···Ag3 (Ag···Ag contact of 2.91 Å) is also identified in MOF **2** and arranged alternatively with that based on Ag1···Ag4 via the Cmdcp ligands to give a 1D chain along the crystallographic *b* direction featuring staggered Ag_4 cubanes (Figures S3e,f). Such a 1D chain further bears Cmdcp ligands project into four directions within the *ac* plane, serving as the eight-connecting node to associate adjacent chains to give a 2D layer extended along the *ab* plane (Figure S3g), with uncoordinated H_2O molecules reside in-between these layers (Figure 3).

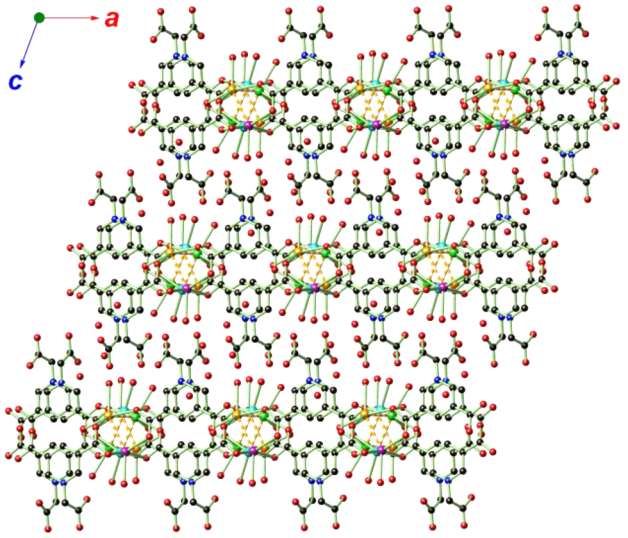

Figure 3. Two-dimensional structure formed from Ag^+ and ligand looking down along the *b* axis. Ag(1) (dark magenta), Ag(2) (cyan), Ag(3) (lime green), Ag(4) (orange) O (red), N (blue), C (black).

Antimicrobial Activity. Antimicrobial activities were measured using a microdilution method. As summarized in Table 1, MOF **2** had a strong antimicrobial activity with a wide antimicrobial spectrum toward normal Gram-positive bacteria, Gram-negative bacteria, and MRSA. Among the tested microorganisms, the activity of MOF **2** was much better than that of the positive control ampicillin and MOF **1**. The *P. acnes* ATCC6919 strain was the most sensitive by MOF **2** with a minimum inhibitory concentration (MIC) of 2.51 μM. The MIC of MOF **2** is 10.04 μM for *E. coli* ATCC25922, *P. asaeruginose* ATCC27853, *S. aureus* ATCC6538, *B. subtilis* CMCC63501, *MRSA* 64589, and *M. albican* ATCC2002, and 5.02 μM for *S. aureus* ATCC25923. Meanwhile, MOF **1** presented with less antimicrobial activity against tested strains except *MRSA* 64589 and *P. acnes* ATCC6919 with both 37.84 μM MIC.

Under similar experimental conditions, the ligands H_3CedcpBr and H_3CmdcpBr with aromatic rings showed no obvious antibacterial activity. In sharp contrast, the activities of both MOFs **1** and **2** were much superior to that of $AgNO_3$. Therefore, we speculate that the main reason for antibacterial action is the synergistic effect from aromatic rings, charge-positive pyridinium, as well as the Ag^+ on the surface of MOFs, and the formation of MOF structure is a necessary condition for the antibacterial activity. Compared with the 3D MOF **1** with larger steric hindrance (Figure 2b), MOF **2** has better antibacterial activity. We reason that MOF **2** featuring 2D, layered structure with low steric hindrance (Figure 3) is more conducive to bacterial adhesion, and Ag^+ exposed to the MOF surface further increases the probability of interaction toward bacterial cell wall.[4] The antibacterial results of MOFs **1** and **2** are shown in Table 1.

Morphological Alterations of Bacterial Cells upon Treatment with 1 and 2. Both MOFs **1** and **2** exhibited significant antimicrobial activity against *S. aureus* ATCC 25923. To clarify the antibacterial mechanisms of the silver-based MOFs against *S. aureus*, its morphological alterations were obtained by SEM. Intact *S. aureus* in Figure 4a and b has

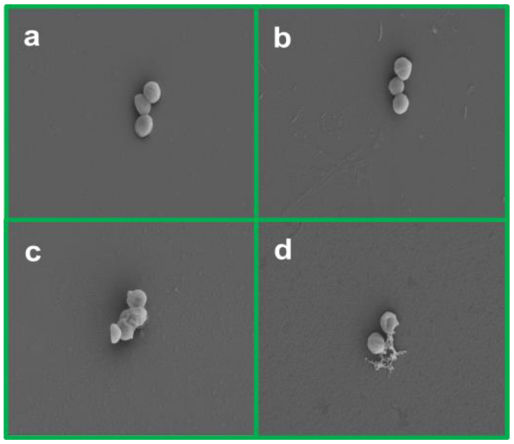

Figure 4. Membrane morphology of *S. aureus* by scanning electron microscopy (SEM) before (a (**1**), b (**2**)) and after (c (**1**), d (**2**)) handled with MOF **1** (1 × MIC) and **2** (1 × MIC).

distinct outer membranes, indicating that the cell structures of the bacteria were well-maintained even under high vacuum and energy electron beam. Nevertheless, when the bacteria were cultured with the presence of MOF **1** or **2**, they lost the cellular

Table 1. Antibacterial Activities for MOFs 1 and 2 and Their Components

	MIC (μM)					
microoganisms	H_3CedcpBr	H_3CmdcpBr	$AgNO_3$	**1**	**2**	ampicillin
E. coli ATCC25922	negative	negative	73.59	>37.84	10.04	12.5
P. asaeruginose ATCC27853	negative	negative	141.17	>37.84	10.04	>200
S. aureus ATCC25923	negative	negative	141.17	37.84	5.02	25
S. aureus ATCC6538	negative	negative	141.17	>37.84	10.04	50
B. subtilis CMCC63501	negative	negative	141.17	>37.84	10.04	200
P. acnes ATCC6919	negative	negative	73.59	37.84	2.51	25
MRSA 64589	negative	negative	294.34	37.84	10.04	>200
M. albican ATCC2002	negative	negative	73.59	>37.84	10.04	>200

https://dx.doi.org/10.1021/acsabm.0c00896
ACS Appl. Bio Mater. 2020, 3, 8525−8531

cohesion with outer membranes heavily damaged. The bacteria went to death as characterized by the outflows of cytoplasm (Figure 4c,d). As a result, the morphology damage levels of MOF **1** is lower than that of MOF **2**.

Killing Kinetics Assay. As shown in Figure 5, at concentrations of 1 × MIC, *S. aureus* ATCC 25923 was

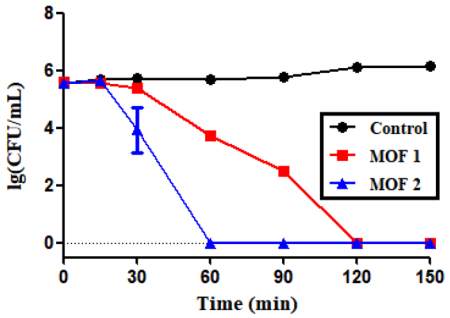

Figure 5. Bactericidal dynamics of MOF **1** and **2** against *S. aureus* ATCC25923.

successfully excluded by MOF **1** or **2** at 120 or 60 min, respectively, without the growing of microbes resuming. The blank control group (no addition of MOF **1** and **2** for coincubation) was used to determine the quantity of *S. aureus* ATCC25923 at 0, 15, 30, 60, 90, 120, and 150 min, respectively. The results showed that the number (Colony-Forming Units, CFU) for bacteria in the control group increased with the extension of time (Figure 5) and MOF **2** can rapidly exert its antibacterial effect than MOF **1**, which may also be related to its 2D planar structure.

Hemolysis Assay. The hemolytic property of MOFs was tested using mouse red blood cells. After 1.5 h of treatment with serial diluted concentrations of MOFs, the morphologies of mice erythrocytes were observed (Figure 6). The results revealed that both MOFs **1** and **2** exhibited a low hemolytic activity against mouse red blood cells. In details, the hemolysis rate of MOF **1** was 2.03 ± 1.08% at a concentration of 37.84 μM, while that of MOF **2** was 6.90 ± 2.34% at a concentration of 10.04 μM (Table 2). All results were compared to the standard control 0.1 M PBS without hemolysis and 0.1% SDS with 100% hemolysis.

CONCLUSION

In this work, we have prepared two Ag-based MOFs $[Ag_2(Cedcp)]_n$ (**1**) and $\{[Ag_4(Cmdcp)_2(H_2O)_4]\cdot 4H_2O\}_n$ (**2**) from the reaction of Ag(I) salts with two pyridinium-dicarboxylic ligands, namely H_3CedcpBr and H_3CmdcpBr. MOF **1** features a 3D framework sustained by a polynuclear silver-cluster, while MOF **2** exhibits a 2D framework layer structure. With a low steric hindrance and the synergistic effect from aromatic ligand backbone coupled with positively charged pyridinium centers, as well as the Ag^+ on its surface, MOF **2** showed superior antibacterial activities with low MIC and rapid responses toward Gramnegative bacteria, Gram-positive bacteria, and fungi. Besides, both MOFs exhibit promising biocompatibility in mice. We hypothesize that the combination of pyridinium-dicarboxylic ligands with Ag(I) to afford synthetic stable and soluble MOF assemblies may pave a new way toward a new class of advanced antibacterial materials.

Table 2. Hemolytic Toxicity for MOFs 1 and 2

1		2	
concentration (μM)	hemolysis ratio (%)	concentration (μM)	hemolysis ratio (%)
37.84	2.03 ± 1.08	10.04	6.90 ± 2.34
18.90	0.39 ± 1.70	5.02	2.21 ± 0.68
9.45	1.56 ± 0.31	2.51	0.45 ± 0.74
4.73	1.24 ± 0.30	1.25	0.78 ± 0.21
2.36	0.58 ± 0.44	0.63	0.65 ± 0.15
1.18	1.54 ± 2.38	0.31	0.46 ± 1.19
0.59	2.76 ± 0.87	0.16	0.29 ± 1.02

ASSOCIATED CONTENT

Supporting Information

The Supporting Information is available free of charge at https://pubs.acs.org/doi/10.1021/acsabm.0c00896.

Selected bond lengths and angles, crystal structure for MOFs **1** and **2**, ^{1}H NMR and ^{13}C NMR for ligand H_3CedcpBr (PDF)

CCDC 2015720 and 2015721, crystallographic data (CIF)

CheckCIF report (PDF)

AUTHOR INFORMATION

Corresponding Authors

Li-Xia Yuan − *School of Chinese Medicine, Southern Medical University, Guangzhou 510515, China*; Email: 195154565@qq.com

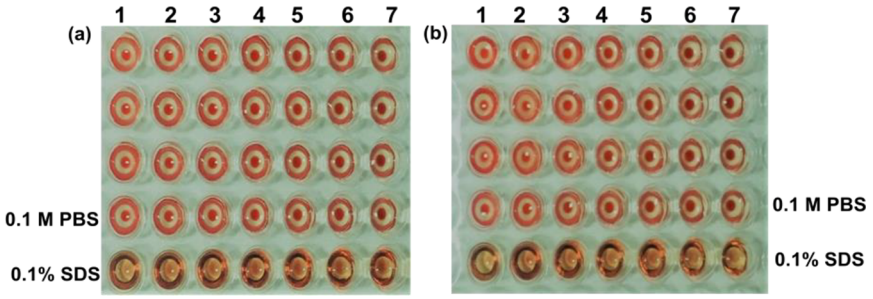

Figure 6. Hemolytic toxicity for MOF **1** (a, lanes 1−7 at the concentrations of 37.84, 18.90, 9.45, 4.73, 2.36, 1.18, 0.59 μM, respectively) and **2** (b, lanes 1−7 at the concentrations of 10.04, 5.02, 2.51, 1.25, 0.63, 0.31, 0.16 μM, respectively). All sample experiments were repeated three times as displayed by the first three lines with the standard control 0.1 M PBS without hemolysis as the fourth line, and 0.1% SDS with 100% hemolysis as the fifth line.

https://dx.doi.org/10.1021/acsabm.0c00896
ACS Appl. Bio Mater. 2020, 3, 8525−8531

Jin-Xiang Chen − *Guangdong Provincial Key Laboratory of New Drug Screening and Guangzhou Key Laboratory of Drug Research for Emerging Virus Prevention and Treatment, Department of Medicinal Chemistry, School of Pharmaceutical Sciences, Southern Medical University, Guangzhou 510515, China;* orcid.org/0000-0002-3963-0718; Email: jxchen@smu.edu.cn

Xue-Qing Xu − *Guangdong Provincial Key Laboratory of New Drug Screening and Guangzhou Key Laboratory of Drug Research for Emerging Virus Prevention and Treatment, Department of Medicinal Chemistry, School of Pharmaceutical Sciences, Southern Medical University, Guangzhou 510515, China;* orcid.org/0000-0002-4525-5803; Email: xu2003@smu.edu.cn

Authors

Bao-Ping Xie − *Guangdong Provincial Key Laboratory of New Drug Screening and Guangzhou Key Laboratory of Drug Research for Emerging Virus Prevention and Treatment, Department of Medicinal Chemistry, School of Pharmaceutical Sciences, Southern Medical University, Guangzhou 510515, China*

Jin-Wei Chai − *Guangdong Provincial Key Laboratory of New Drug Screening and Guangzhou Key Laboratory of Drug Research for Emerging Virus Prevention and Treatment, Department of Medicinal Chemistry, School of Pharmaceutical Sciences, Southern Medical University, Guangzhou 510515, China*

Cheng Fan − *Guangdong Provincial Key Laboratory of New Drug Screening and Guangzhou Key Laboratory of Drug Research for Emerging Virus Prevention and Treatment, Department of Medicinal Chemistry, School of Pharmaceutical Sciences, Southern Medical University, Guangzhou 510515, China*

Ji-Hua Ouyang − *Guangdong Provincial Key Laboratory of New Drug Screening and Guangzhou Key Laboratory of Drug Research for Emerging Virus Prevention and Treatment, Department of Medicinal Chemistry, School of Pharmaceutical Sciences, Southern Medical University, Guangzhou 510515, China*

Wen-Jun Duan − *Guangdong Provincial Key Laboratory of New Drug Screening and Guangzhou Key Laboratory of Drug Research for Emerging Virus Prevention and Treatment, Department of Medicinal Chemistry, School of Pharmaceutical Sciences, Southern Medical University, Guangzhou 510515, China;* orcid.org/0000-0002-9117-7447

Bin Sun − *Guangdong Provincial Key Laboratory of New Drug Screening and Guangzhou Key Laboratory of Drug Research for Emerging Virus Prevention and Treatment, Department of Medicinal Chemistry, School of Pharmaceutical Sciences, Southern Medical University, Guangzhou 510515, China;* orcid.org/0000-0001-6086-0975

Jun Chen − *Guangdong Provincial Key Laboratory of New Drug Screening and Guangzhou Key Laboratory of Drug Research for Emerging Virus Prevention and Treatment, Department of Medicinal Chemistry, School of Pharmaceutical Sciences, Southern Medical University, Guangzhou 510515, China*

Complete contact information is available at: https://pubs.acs.org/10.1021/acsabm.0c00896

Author Contributions

§B.-P.X. and J.-W.C. contributed equally to this work.

Notes

The authors declare no competing financial interest.

■ ACKNOWLEDGMENTS

We acknowledge the financial support from the National Natural Science Foundation (NNSF) of China (21874064), the Natural Science Foundation form Guangdong Science and Technology Department of China (2018A030313456), Science and Technology Program of Guangzhou (201904010410), and the One Belt One Road Incubation Project funded by Southern Medical University (YD2018N003).

■ REFERENCES

(1) Laxminarayan, R.; Matsoso, P.; Pant, S.; Brower, C.; Røttingen, J.-A.; Klugman, K.; Davies, S. Access to Effective Antimicrobials: A Worldwide Challenge. *Lancet* **2016**, *387*, 168−175.

(2) Berendonk, T. U.; Manaia, C. M.; Merlin, C.; Fatta, K. D.; Cytryn, E.; Walsh, F.; et al. Tackling Antibiotic Resistance: The Environmental Framework. *Nat. Rev. Microbiol.* **2015**, *13*, 310−317.

(3) Zhang, Y.; Chen, Y.; Zhang, H.; Zhang, B.; Liu, J. Potent Antibacterial Activity of A Novel Silver Nanoparticle-halloysite Nanotube Nanocomposite Powder. *J. Inorg. Biochem.* **2013**, *118*, 59−64.

(4) Song, H. Y.; Kim, M. R.; Lee, M. J.; Jeon, E. S.; Bae, Y. C.; Jung, J. S.; et al. Oncostatin M Decreases Adiponectin Expression and Induces Dedifferentiation of Adipocytes by JAK3- and MEK-dependent Pathways. *Int. J. Biochem. Cell Biol.* **2007**, *39*, 439−449.

(5) Zhu, X. Q.; Zhu, Y. N.; Jia, K.; Abraha, B. S.; Li, Y.; Peng, W. C.; Zhang, F. B.; Fan, X. B.; Zhang, L. A Near-Infrared Light-Mediated Antimicrobial Based on Ag/$Ti_3C_2T_x$ for Effective Synergetic Antibacterial Applications. *Nanoscale* **2020**, *12*, 19129−19141.

(6) Gao, L. H.; Wang, Y. W.; Li, Y. M.; Xu, M. X.; Sun, G.; Zou, T.; Wang, F. J.; Xu, S. J.; Da, J.; Wang, L. Biomimetic Biodegradable Ag@Au Nanoparticle-Embedded Ureteral Stent with a Constantly Renewable Contact-Killing Antimicrobial Surface and Antibiofilm and Extraction-Free Properties. *Acta Biomater.* **2020**, *114*, 117−132.

(7) Xie, X. L.; Sun, T. C.; Xue, J. Z.; Miao, Z. H.; Yan, X.; Fang, W. W.; Li, Q.; Tang, R. P.; Lu, Y.; Tang, L. X.; Zha, Z. B.; He, T. Ag Nanoparticles Cluster with pH-Triggered Reassembly in Targeting Antimicrobial Applications. *Adv. Funct. Mater.* **2020**, *30*, 2000511.

(8) Wiechers, J. W.; Musee, N. Engineered Inorganic Nanoparticles and Cosmetics: Facts, Issues, Knowledge Gaps and Challenges. *J. Biomed. Nanotechnol.* **2010**, *6*, 408−431.

(9) Lu, X.; Ye, J.; Zhang, D.; Xie, R.; Bogale, R. F.; Sun, Y.; et al. Silver Carboxylate Metal-Organic Frameworks With Highly Antibacterial Activity and Biocompatibility. *J. Inorg. Biochem.* **2014**, *138*, 114−121.

(10) Jo, J. H.; Kim, H. C.; Huh, S.; Kim, Y.; Lee, D. N. Antibacterial Activities of Cu-MOFs Containing Glutarates and Bipyridyl Ligands. *Dalton Trans.* **2019**, *48*, 8084−8093.

(11) Sava Gallis, D. F.; Butler, K. S.; Agola, J. O.; Pearce, C. J.; McBride, A. A. Antibacterial Countermeasures via Metal-Organic Framework Supported Sustained Therapeutic Release. *ACS Appl. Mater. Interfaces* **2019**, *11*, 7782−7791.

(12) Singbumrung, K.; Motina, K.; Pisitsak, P.; Chitichotpanya, P.; Wongkasemjit, S.; Inprasit, T. Preparation of Cu-BTC/PVA Fibers with Antibacterial Applications. *Fibers Polym.* **2018**, *19*, 1373−1378.

(13) Wang, X. S.; Chen, C. H.; Ichihara, F.; Oshikiri, M.; Liang, J.; Li, L.; Li, Y. X.; Song, H.; Wang, S. Y.; Zhang, T.; Huang, Y. B.; Cao, R.; Ye, J. H. Integration of Adsorption and Photosensitivity Capabilities into a Cationic Multivariate Metal-Organic Framework for Enhanced Visible-Light Photoreduction Reaction. *Appl. Catal., B* **2019**, *253*, 323−330.

(14) Abd El Salam, H. M.; Nassar, H. N.; Khidr, A. S. A.; Zaki, T. Antimicrobial Activities of Green Synthesized Ag Nanoparticles@Ni-MOF Nanosheets. *J. Inorg. Organomet. Polym. Mater.* **2018**, *28*, 2791−2798.
(15) Nomiya, K.; Tsuda, K.; Sudoh, T.; Oda, M. Ag(I)-N Bond-Containing Compound Showing Wide Spectra in Effective Antimicrobial Activities: Polymeric Silver(I) Imidazolate. *J. Inorg. Biochem.* **1997**, *68*, 39−44.
(16) Tamames-Tabar, C.; Imbuluzqueta, E.; Guillou, N.; Serre, C.; Miller, S. R.; Elkaim, E.; Horcajada, P.; Blanco-Prieto, M. J. A Zn Azelate MOF: Combining Antibacterial Effect. *CrystEngComm* **2015**, *17*, 456−462.
(17) Shakya, S.; He, Y. P.; Ren, X. H.; Guo, T.; Maharjan, A.; Luo, T.; Wang, T. T.; Dhakhwa, R.; Regmi, B.; Li, H. Y.; Gref, R.; Zhang, J. W. Ultrafine Silver Nanoparticles Embedded in Cyclodextrin Metal-Organic Frameworks with GRGDS Functionalization to Promote Antibacterial and Wound Healing Application. *Small* **2019**, *15*, e1901065.
(18) Qin, L.; Sun, Z. Y.; Cheng, K.; Liu, S. W.; Pang, J. X.; Xia, L. M.; Chen, W. H.; Cheng, Z.; Chen, J. X. Zwitterionic Manganes and Gadolinium Metal-Organic Frameworks as Efficient Magnetic Resonance Contrast Agents for in Vivo Imaging. *ACS Appl. Mater. Interfaces* **2017**, *9*, 41378−41386.
(19) Xie, B. P.; Qiu, G. H.; Sun, B.; Yang, Z. F.; Zhang, W. H.; Chen, J. X.; Jiang, Z. H. Synchronous Sensing of Three Conserved Sequences of Zika Virus by a DNAs@MOF Hybrid: Experimental and Molecular Simulation Studies. *Inorg. Chem. Front.* **2019**, *6*, 148−152.
(20) Lin, S.-X.; Pan, W.-L.; Niu, R.-J.; Liu, Y.; Chen, J.-X.; Zhang, W.-H.; Lang, J.-P.; Young, D. J. Effective Loading of Cisplatin into a Nanoscale UiO-66 Metal-Organic Framework with Preformed Defects. *Dalton Trans.* **2019**, *48*, 5308−5314.
(21) Huang, N. H.; Li, R. T.; Fan, C.; Wu, K. Y.; Zhang, Z.; Chen, J. X. Rapid Sequential Detection of Hg^{2+} and Biothiols by a Probe DNA-MOF Hybrid Sensory System. *J. Inorg. Biochem.* **2019**, *197*, 110690.
(22) Zhai, L. Y.; Li, M. X.; Pan, W. L.; Chen, Y.; Li, M. M.; Pang, J. X.; Zheng, L.; Chen, J. X.; Duan, W. J. In Situ Detection of Plasma Exosomal MicroRNA-1246 for Breast Cancer Diagnostics by a Au Nanoflare Probe. *ACS Appl. Mater. Interfaces* **2018**, *10*, 39478−39486.
(23) Hu, P. P.; Liu, N.; Wu, K. Y.; Zhai, L. Y.; Xie, B. P.; Sun, B.; Duan, W. J.; Zhang, W. H.; Chen, J. X. Successive and Specific Detection of Hg^{2+} and I^- by a DNA@MOF Biosensor: Experimental and Simulation Studies. *Inorg. Chem.* **2018**, *57*, 8382−8389.
(24) Cai, S. L.; Yang, Z. C.; Wu, K. Y.; Fan, C.; Zhai, L. Y.; Huang, N. H.; Li, R. T.; Duan, W. J.; Chen, J. X. Experimental and Computational Investigation of a DNA-Shielded 3D Metal-Organic Framework for the Prompt Dual Sensing of Ag^+ and S^{2-}. *RSC Adv.* **2019**, *9*, 15424−15430.
(25) Wu, K. Y.; Qin, L.; Fan, C.; Cai, S. L.; Zhang, T. T.; Chen, W. H.; Tang, X. Y.; Chen, J. X. Sequential and Recyclable Sensing of Fe^{3+} and Ascorbic Acid Based on a Water-stable Green-emitting Terbium-(III) Metal-Organic Framework. *Dalton Trans.* **2019**, *48*, 8911−8919.
(26) Chen, J. X.; Zhao, H. Q.; Li, H. H.; Huang, S. L.; Ding, N. N.; Chen, W. H.; Young, D. J.; Zhang, W. H.; Andy Hor, T. S. Bent Tritopic Carboxylates for Coordination Networks: Clues to the Origin of Self-penetration. *CrystEngComm* **2014**, *16*, 7722−7730.
(27) Sheldrick, G. M. *SADABS. Program for Empirical Adsorption Correction of Area Detector Data*; University of Göttingen: Göttingen, Germany, 1996.
(28) Sheldrick, G. M. Crystal Structure Refinement with SHELXL. *Acta Crystallogr., Sect. C: Struct. Chem.* **2015**, *71*, 3−8.
(29) Farrugia, L. J. WinGX Suite for Small-Molecule Single-Crystal Crystallography. *J. Appl. Crystallogr.* **1999**, *32*, 837−838.
(30) Zeng, B. S.; Chai, J. W.; Deng, Z. H.; Ye, T. F.; Chen, W. B.; Li, D.; Chen, X.; Chen, M.; Xu, X. Q. Functional Characterization of a Novel Lipopolysaccharide-Binding Antimicrobial and Anti-inflammatory Peptide in Vitro and in Vivo. *J. Med. Chem.* **2018**, *61*, 10709−10723.
(31) Pejman, M.; Firouzjaei, M. D.; Aktij, S. A.; Das, P.; T iraferri, A.; et al. In Situ Ag-MOF Growth on Pre-grafted Zwitterions Imparts Outstanding Antifouling Properties to Forward Osmosis Membranes. *ACS Appl. Mater. Interfaces* **2020**, *32*, 36287−36300.
(32) Hao, Z. M.; Chao, M. Y.; Liu, Y.; Song, Y. L.; Yang, J. Y.; Ding, L. F.; Zhang, W. H.; Lang, J. P. Evaluating the Component Contribution to Nonlinear Optical Performances Using Stable $[Ni_4O_4]$ Cuboidal Clusters as Models. *Dalton Trans.* **2018**, *47*, 8865−8869.

NOTE ADDED AFTER ASAP PUBLICATION

This paper was published ASAP on November 11, 2020 with missing designation and contact information for corresponding author Li-Xia Yuan. The corrected version was posted November 30, 2020.

https://dx.doi.org/10.1021/acsabm.0c00896
ACS Appl. Bio Mater. 2020, 3, 8525−8531